JOURNAL OF APPLIED ELECTROCHEMISTRY 17 (1987) 1118–1128

# *Mass transfer downstream of nozzles in turbulent pipe flow with varying Schmidt number*

S. M. CHOUIKHI*, M. A. PATRICK, A. A. WRAGG†

*Department of Chemical Engineering, University of Exeter, Exeter EX4 4QF, UK*

Received 10 February 1987; revised 18 March 1987

Local mass transfer rates at the wall of a pipe downstream of constricting nozzles have been measured using the electrochemical limiting diffusion current technique for different electrolyte Schmidt numbers. The familiar peaked axial distribution of mass transfer downstream of the nozzle was verified and the peak mass transfer values were found to agree well with the data of Tagg *et al.* [1]. An overall correlation of the data in terms of both Reynolds number and nozzle expansion ratio produced the equation

$$(Sh_{2P}/Sh_{2FD})(D_1/D_2)^{-0.7} = 14.39\ Re_2^{-0.182}$$

Limiting current–time traces produced evidence of the highly turbulent flow in the recirculation zone near the position of peak mass transfer.

**Nomenclature**

$A$ electrode surface area
$D$ diameter
$\mathscr{D}$ diffusion coefficient
$C$ bulk concentration of $Fe(CN)_6^{3-}$
$F$ Faraday number
$I_L$ limiting current
$k$ mass transfer coefficient
$u$ liquid velocity
$x$ distance downstream of nozzle

*Greek symbols*

$\mu$ dynamic viscosity
$\varrho$ density

*Dimensionless groups*

$Re$ Reynolds number, $Du\varrho/\mu$
$Sc$ Schmidt number, $\mu/\varrho\mathscr{D}$
$Sh$ Sherwood number, $kD/\mathscr{D}$

*Subscripts*

1 nozzle
2 downstream pipe
FD fully developed
P peak (maximum) value

## 1. Introduction

There is considerable interest in transport processes downstream of obstructions in pipe lines since a complex hydrodynamic region exists involving separation, recirculation and reattachment of the flow in the immediate downstream region. This zone of complex flow is associated with enhanced rates of heat and/or mass transfer between the fluid and the duct walls and may also be associated with severe corrosion problems. This type of flow situation may be found in the immediate vicinity of valves, orifices, nozzles, boiler tube gags and sudden changes of pipeline diameter and may also be encountered in the region adjacent to electrochemical cell inlet ports.

Earlier work in these laboratories [1] involved measurements of mass transfer at micro-electrodes situated in a pipe wall immediately downstream of profiled nozzles giving expansion ratios of 2, 3, 4, 6 and 10. The limiting current

* *Present address*: AFRC Institute of Food Research, Norwich Laboratory, Colney Lane, Norwich NR4 7UA, UK.
† To whom correspondence should be addressed.



0021–891X/87 $03.00 + .12 

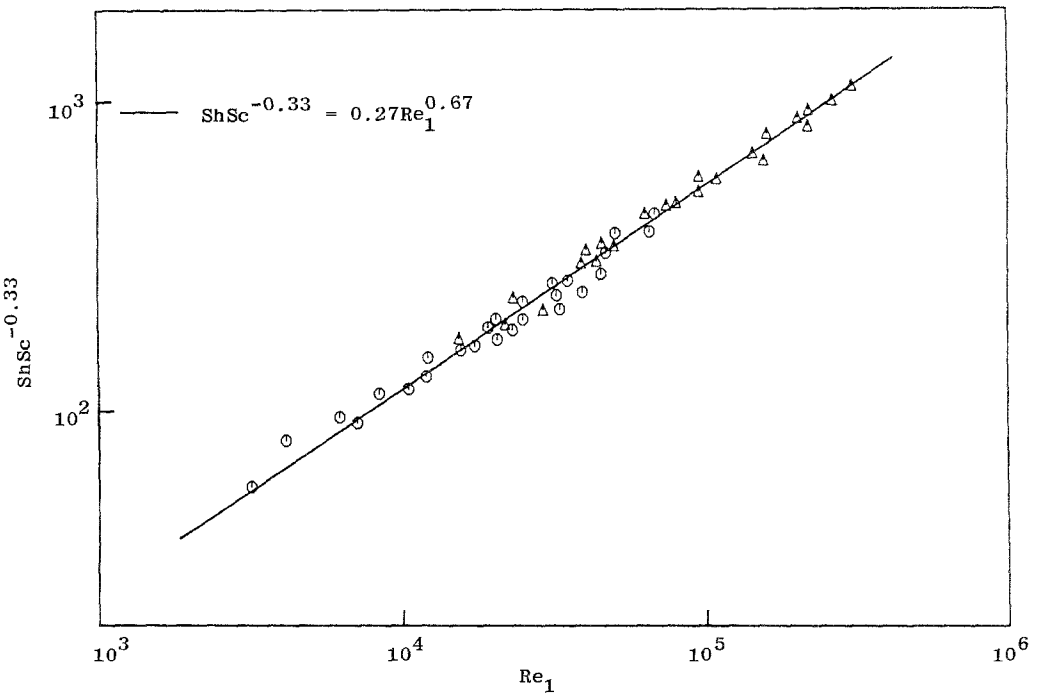


Fig. 1. Comparison and correlation of peak mass transfer and heat transfer data downstream of pipe line constrictions according to (○) Tagg *et al.* [1] and (△) Krall and Sparrow [2].

technique was employed using the cathodic reduction of ferricyanide ions at nickel electrodes. The peak valves of local mass transfer rate were correlated successfully by the equation

$$Sh_p = 0.27Re_1^{0.67}Sc^{0.33} \quad (1)$$

and the data were found to be in excellent agreement with the heat transfer results of Krall and Sparrow [2] when expressed via the Chilton–Colburn analogy between heat and mass transfer. Krall and Sparrow used an electrically heated tube downstream of an orifice with water as the working fluid. Thus, mass transfer data at a property number (Schmidt number) of $\approx 1500$ could be correlated along with heat transfer data at a property number (Prandtl number between 3 and 6), as illustrated in Fig. 1. This finding is of considerable importance to the modelling of heat transfer processes using mass transfer analogues and it was felt to be necessary to corroborate the results of Tagg *et al.* in a completely reconstructed apparatus and independent programme of work. The present work was therefore carried out as part of a study of two-phase (gas–liquid) flows through nozzles [3] and involved shear stress, recirculation zone length and mass transfer distribution measurements; hydrodynamic and two-phase mass transfer results have been published elsewhere [4, 5]. In the present programmes of work the Schmidt number of the electrolyte was varied by the use of supporting electrolyte of different strengths.

The purpose of the present work was, therefore, three fold; namely, to corroborate the data of Tagg *et al.* [1], to provide a single-phase datum against which to analyse mass transfer data for two-phase flow [5], and to investigate the effect of varying Schmidt number.

Further noteworthy electrochemical investigations of similar complex flows have been carried out by Runchal [6] who worked with a sudden 1 : 2 pipe line expansion, and Sydberger and Lotz [7] who worked with a segmented nickel cathode downstream of orifices and circumferential slots. Harris [8] has also made a comparative study of the region downstream of orifices and ferrules. Related work, but using a plaster dissolution technique, was carried out by Wilkin and Cheung [9]. This latter technique produces a change in the duct surface profile in

the region of enhanced dissolution. Poulson and Robinson [10] have also described measurements of mass transfer–corrosion downstream of orifices using copper pipes exposed to an aqueous solution of ferric chloride. Again, the pipe profile changes in the region of enhanced mass transfer, control of the process being due to ferric ion transfer to the wall.

Both Wragg *et al.* [11] and Awe *et al.* [12] have investigated the problem of expansions from circular constrictions to square downstream sections. In both these studies the distribution of mass transfer was measured, Wragg *et al.* using 1 mm diameter nickel micro-electrodes in nickel plate duct walls and Awe *et al.* using copper strips 50 mm long so that less detailed mapping was obtained. Wragg *et al.* also studied the spanwise distribution of mass transfer on the cell walls.

In all the foregoing studies a pronounced peak in the mass–heat transfer distribution has been obtained immediately downstream of the flow obstruction, in some cases amounting to more than 10 times the magnitude of the fully developed value. This highlights the susceptibility to enhanced corrosion in flowing fluids in such geometries where there is some degree of mass transfer control of the process. Poulson [13] has contributed a significant review exploring the relationship between flow and corrosion in which some of the previous studies are critically evaluated.

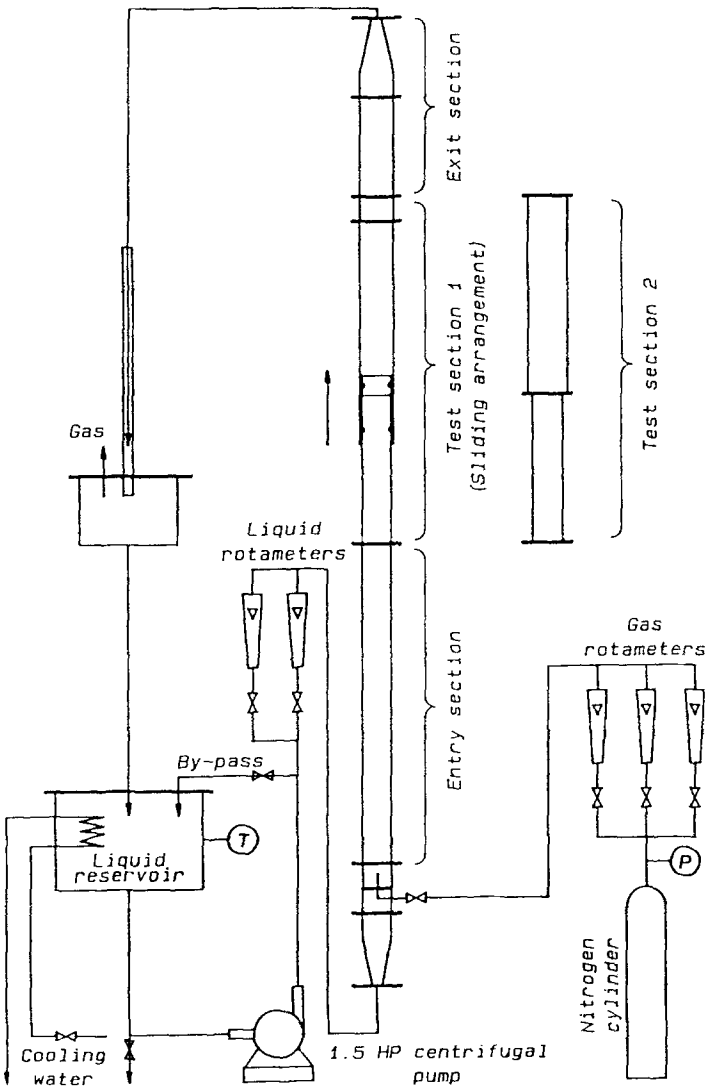


Fig. 2. Diagram of flow rig.

## 2. Experimental details

The flow rig is depicted in Fig. 2. The nitrogen supply and injection facility was used in the associated two-phase flow work but not in that described here. A 1.5 HP pump maintained a supply of electrolyte to a 42 mm i.d. PVC pipe via a bank of rotameters, a flow straightener and a diffuser. The flow development section (entry section) was 50 pipe diameters long.

Two test sections could be used in this rig. The first (test section 1) was an axially divided Perspex tube which was equipped with two nickel micro-electrodes and a dual element (sandwich) electrode. The positions of these electrodes with respect to the nozzle expansion at the test section entry could be varied by means of a double 'O' ring sealed sliding arrangement. This is described in detail elsewhere [3] and shear stress and recirculation zone length measurements have been reported [4]. The second test section was used for the mass transfer measurements in both single- and two-phase flow and was made from a 50.8 mm i.d. schedule 80 Nickel tube of length 510 mm and fitted with stainless steel flanges. The tube was bored to 51.0 mm i.d. and then split axially giving an area ratio of 2 : 1, the smaller part being used as the macrocathode to ensure that the mass transfer process was cathode limited. Two rows of 32 holes, 1.2 mm in diameter, were drilled in the cathode to house the local cathodes which were of nickel wire (99.98%), 1 mm in diameter. The microcathodes were fixed and insulated from the main cathode using Araldite 2004, the nominal insulation thickness being 0.1 mm, and the inside ends were ground and polished flush with the pipe wall. The protruding back ends of the microelectrodes were protected by a Perspex backing cap and connected individually by two 32-way sockets. The two sections of the nickel pipe were held together by two outer PVC flanges and the gap between them was filled with Araldite 2004.

A selected ASME long radius nozzle was inserted at the upstream end of the test section, the first local mass transfer measurement being at a distance 0.0625 $D_2$ from the nozzle. The remaining electrodes were situated at spacings of 0.127 $D_2$ in the axial direction.

Fig. 3 gives details of the electrical circuit and instrumentation used. The main and microcathodes were maintained at the same potential and a voltage of $\approx 800$ mV was supplied between anode and cathode, a value known to correspond to the mid-plateau region of the current–voltage curves. Limiting currents were measured using a 32-channel data acquisition system built in-house [14] which was capable of averaging

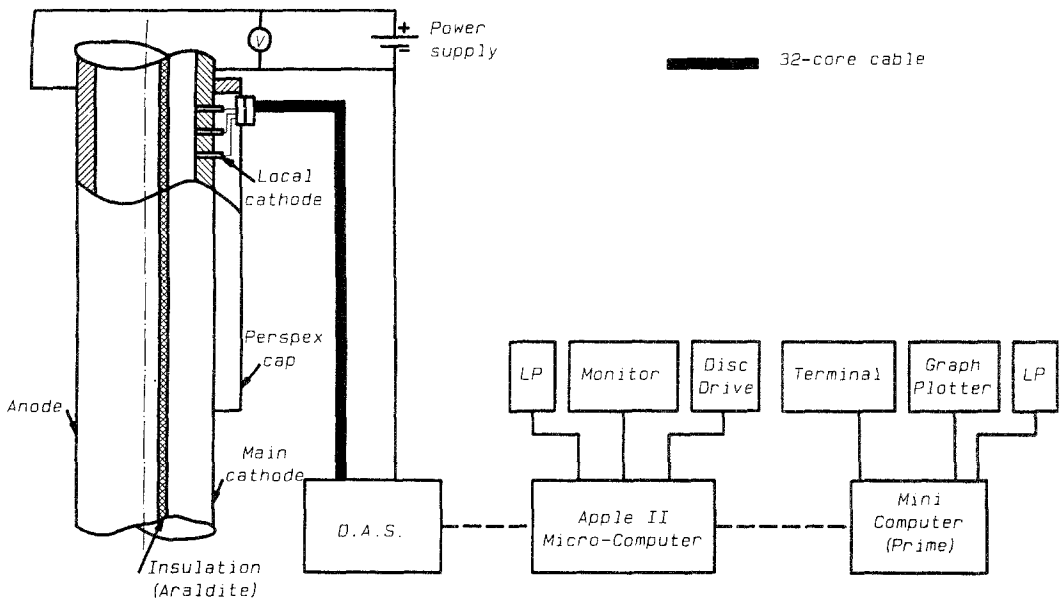


Fig. 3. Arrangement of electrodes and instrumentation.

*Table 1. Composition and physical properties of the electrolytes*

| | *Solution* | | |
|---|---|---|---|
| | *1* | *2* | *3* |
| Concentration of $Fe(CN)_6^{-3}$ (M) | ~0.005 | ~0.005 | ~0.005 |
| Concentration of $Fe(CN)_6^{-4}$ (M) | ~0.005 | ~0.005 | ~0.005 |
| Concentration of NaOH (M) | 0.5 | 2.0 | 3.0 |
| Density, $\varrho$ ($kg\,m^{-3}$) | 1020 | 1080.2 | 1117.17 |
| Viscosity, $\mu$ ($kg\,m^{-1}\,s^{-1}$) | $1.1078 \times 10^{-3}$ | $1.5608 \times 10^{-3}$ | $1.9634 \times 10^{-3}$ |
| Diffusivity, $\mathscr{D}$ ($m^2\,s^{-1}$) | $6.6123 \times 10^{-10}$ | $4.6931 \times 10^{-10}$ | $3.7306 \times 10^{-10}$ |
| *Sc* | 1640 | 3070 | 4710 |

the fluctuating signals from up to 32 channels scanned at a frequency of 100 Hz over a period of 60 s.

The electrolyte was an aqueous equimolar mixture of potassium ferri- and ferro-cyanides with varying concentrations of sodium hydroxide as supporting electrolyte. The compositions and physical properties of the electrolytes used

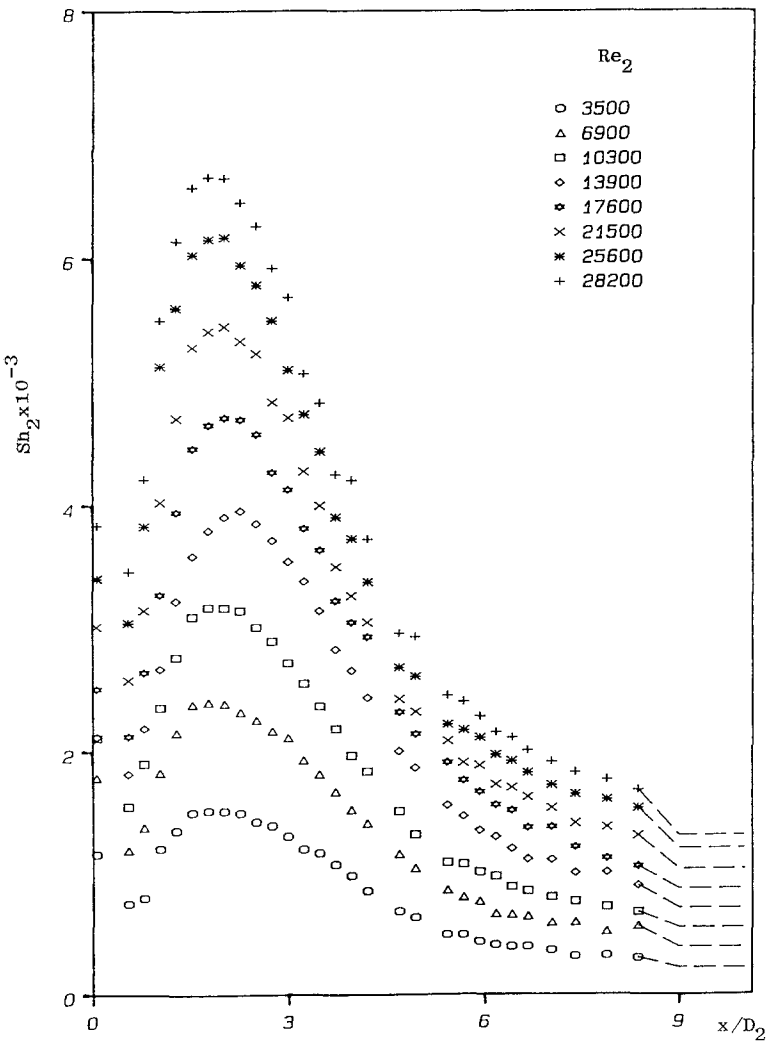


Fig. 4. Axial mass transfer distribution downstream of the nozzle expansion $D_1 : D_2 = 1 : 3$, for $Sc = 1640$.

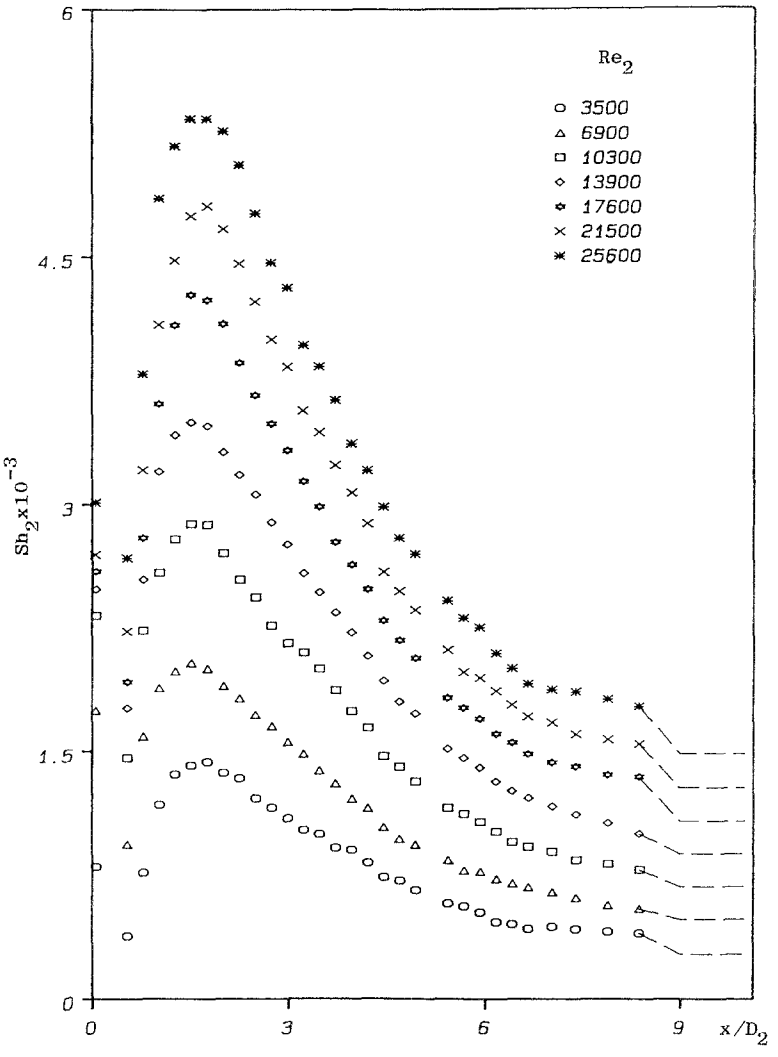


Fig. 5. Axial mass transfer distribution downstream of the nozzle expansion $D_1 : D_2 = 1:2$, for $Sc = 3070$.

are given in Table 1. The electrolyte was deoxygenated by continuous $N_2$ bubbling in the bulk tank and the maintenance of a $N_2$ blanket at all times. The temperature was maintained at $20 \pm 0.5°C$ by means of a water-cooled glass cooling coil. The ferricyanide ion concentration was measured prior to and following each day's tests by UV spectrophotometry.

The use of the limiting current technique in mass transfer measurement is described and reviewed elsewhere [15, 16].

## 3. Results and discussion

Typical distributions of local mass transfer downstream of the nozzles are shown as plots of Sherwood number against non-dimensional downstream distance in Figs 4, 5 and 6. Results from one row of electrodes only are presented for clarity. A full set of such results for all nozzles and all Schmidt numbers is available elsewhere [3]. All the curves show a distinct minimum immediately downstream of the nozzle at the second micro-electrode. This is associated with the small secondary recirculation zone previously identified by Tagg *et al.* [1]. All the curves then display a very marked maximum, or peak, associated with the main recirculation zone before gradually asymptoting to a fully developed far-downstream value. The horizontal broken line at the far right of each curve in Figs 4 to 6 represents the anticipated

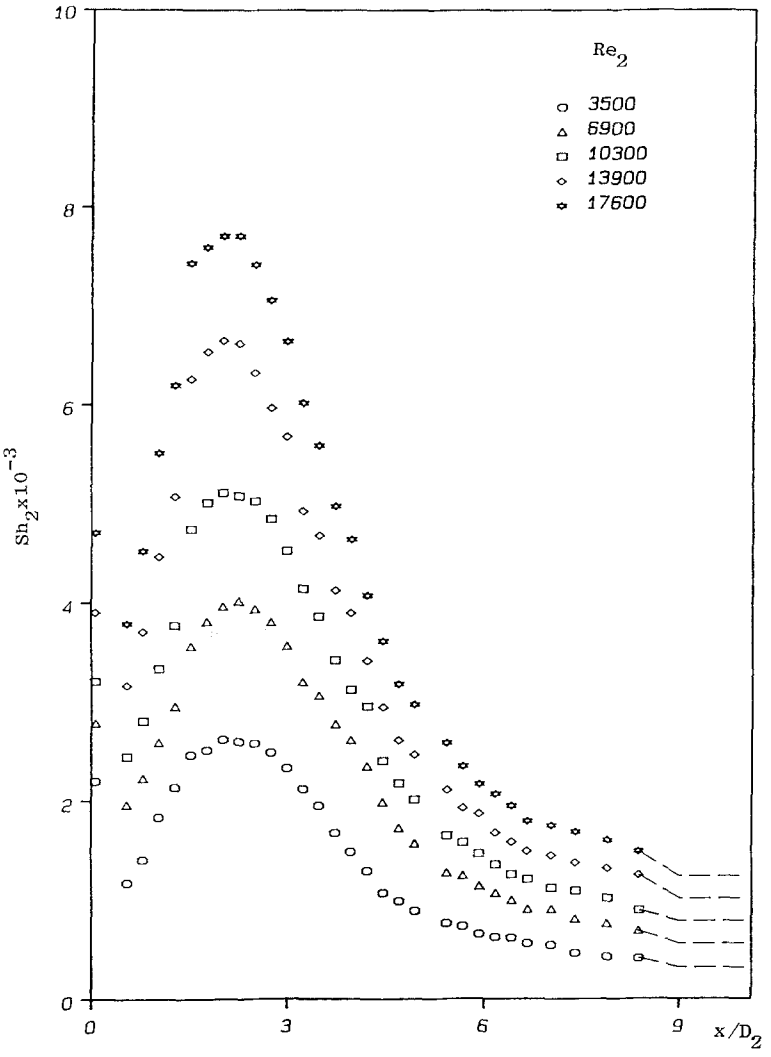


Fig. 6. Axial mass transfer distribution downstream of the nozzle expansion $D_1 : D_2 = 1 : 4$, for $Sc = 4710$.

fully developed value of $Sh_2$ for a pipe as given by the equation of Berger and Hau [17]:

$$Sh_{FD} = 0.0165\, Re_2^{0.86} Sc^{0.33} \quad (2)$$

From the curves shown in Figs 4 to 6 (and the similar figures for other nozzles and Schmidt numbers [3]) the maximum, or peak, values of Sherwood number were estimated. Fig. 7 shows a plot of the peak Sherwood numbers against nozzle Reynolds number from which it is seen that the data for different Schmidt numbers fall on distinct straight lines for which the best fit correlations gave:

$$Sh_{2P} = 2.40 Re_1^{0.697} \quad \text{for } Sc = 1640 \quad (3)$$

$$Sh_{2P} = 2.80 Re_1^{0.698} \quad \text{for } Sc = 3070 \quad (4)$$

$$Sh_{2P} = 4.33 Re_1^{0.67} \quad \text{for } Sc = 4710 \quad (5)$$

It can be seen that the value of the exponent on $Re_1$ is in good agreement with that of 0.67 found by Krall and Sparrow [2] for heat transfer and by Tagg *et al.* [1] in the earlier mass transfer study. Fig. 8 is a plot of $Sh_{2P} Sc^{-0.33}$ against $Re_1$ which brings together all the results from the different Schmidt numbers and also compares the data with the previous correlation of Tagg *et al.* [1]. It is apparent that good agreement is obtained and that the present results constitute a valuable corroboration of those of Tagg and confirm the heat–mass transfer analogy implications.

Fig. 9 shows a plot of the maximum local

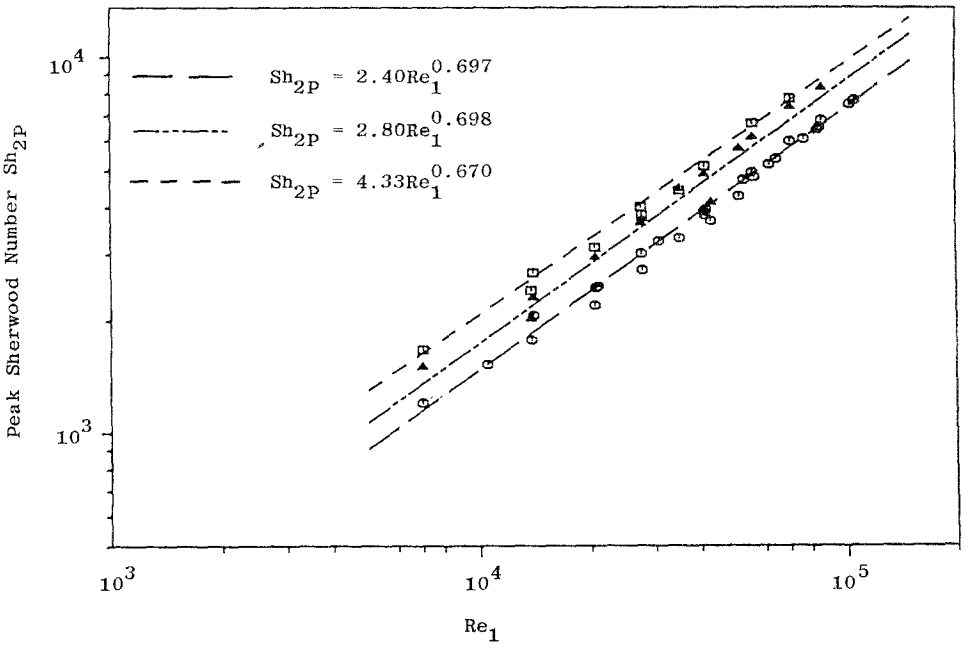


Fig. 7. Correlation of peak mass transfer coefficients for each Schmidt number. Values of $Sc$: (○) 1640; (▲) 3070; (□) 4710.

mass transfer enhancement, $Sh_{2P}/Sh_{2FD}$, as a function of downstream Reynolds number for each expansion ratio and property number investigated. It can be seen that the mass transfer enhancement, while being essentially independent of electrolyte property number, is dependent on both the expansion ratio and on the downstream Reynolds number, $Re_2$. The mass transfer enhancement is highest for the highest expansion ratio, the enhancement factor being of the order of 10 at the lower Reynolds numbers. This highlights the vulnerability of

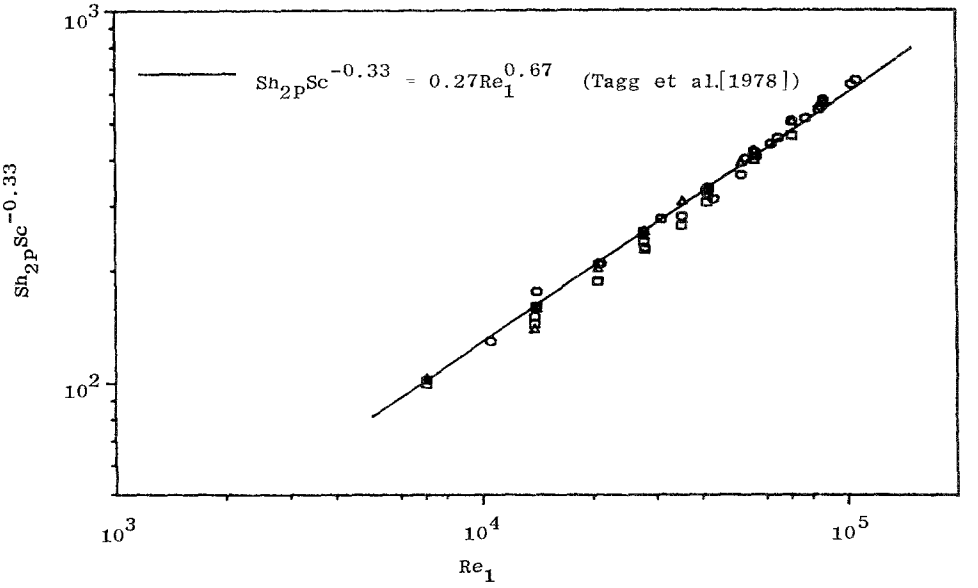


Fig. 8. Overall correlation of peak mass transfer coefficients and comparison with the correlation of Tagg *et al.* [1]. Values of $Sc$: (○) 1640; (△) 3070; (□) 4710.

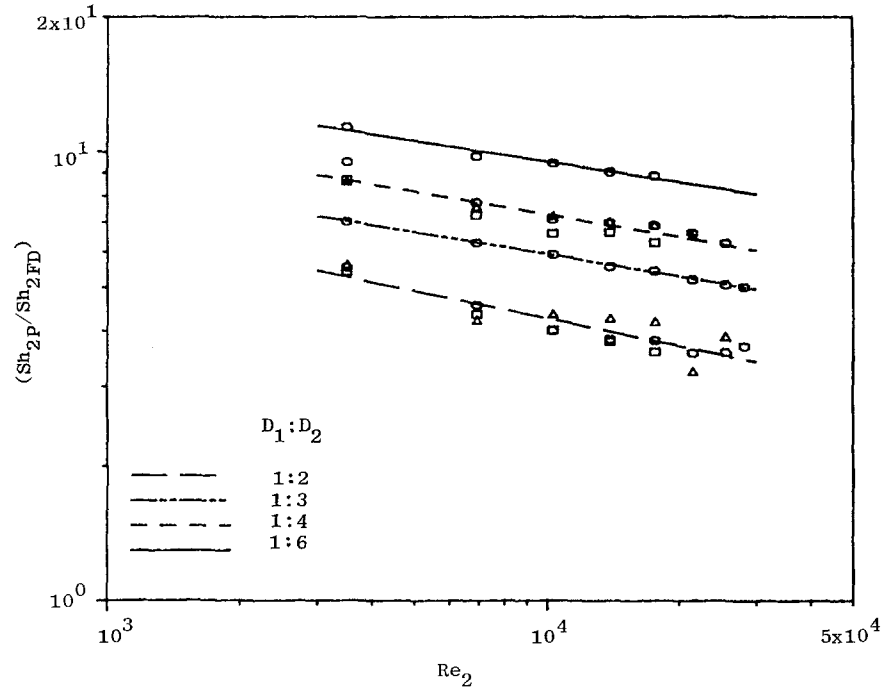


Fig. 9. Enhancement of local mass transfer above fully developed downstream value. $Sh_{2FD}$ was calculated via the Berger and Hau equation, $Sh_{2FD} = 0.0165 Re_2^{0.86} Sc^{-0.33}$ [17]. Values of $Sc$ as for Fig. 8.

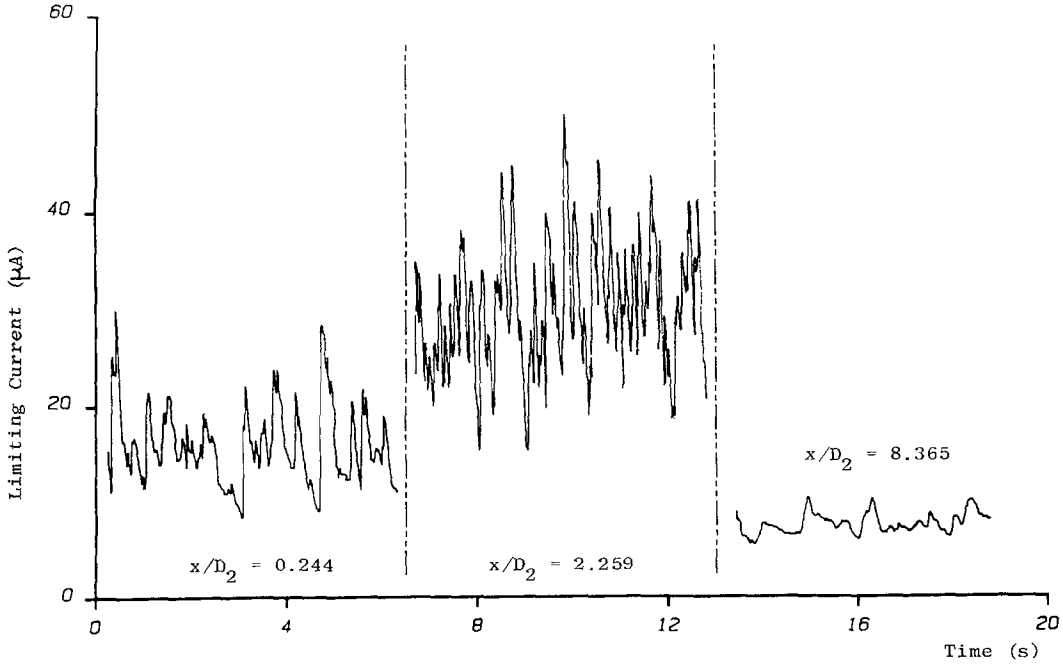


Fig. 10. Limiting current fluctuations downstream of the nozzle expansion $D_1 : D_2 = 1 : 3$. $Sc = 1640$.

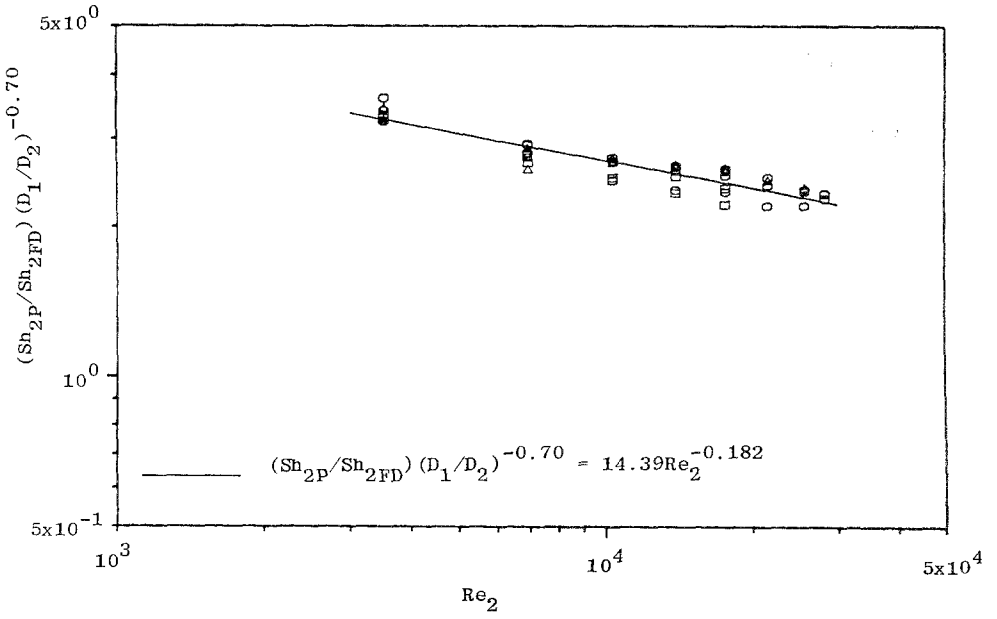


Fig. 11. Overall correlation of peak mass transfer rates in terms of fully developed values for all nozzles. Values of *Sc* as for Fig. 8.

pipe walls to flow-related corrosion problems downstream of obstructions producing complex flows.

The enhancing of mass transfer due to turbulence in the recirculation zone downstream of the nozzle is well illustrated by the limiting current versus time traces depicted in Fig. 10. The second trace at $x/D_2 = 2.259$, close to the peak mass transfer position, shows fluctuations of high amplitude and frequency, indicative of the intense turbulence at this point. In contrast, the trace at $x/D_2 = 8.365$, well into the redevelopment zone, shows much less turbulence.

Fig. 11 shows a reasonably successful attempt to correlate peak transfer rates normalized with respect to fully developed values in terms of both Reynolds number and expansion ratio. The equation of the best fit line through the points is

$$(Sh_{2P}/Sh_{2FD})(D_1/D_2)^{-0.7} = 14.39Re_2^{-0.182} \quad (6)$$

It is thus possible to predict the anticipated maximum enhancement of mass or heat transfer rate downstream of any nozzle with reasonable accuracy and it is expected that other types of axysymmetric constriction would produce similar behaviour.

The significant effects of introducing a second phase (gaseous nitrogen) into the flow prior to the nozzle has also been thoroughly investigated by the authors and the resultant mass transfer distributions are reported elsewhere [3, 5].

## Acknowledgement

Financial support of this work by the United Kingdom Atomic Energy Authority, AEE, Winfrith, Dorset, is gratefully acknowledged.

## References

[1] D. J. Tagg, M. A. Patrick and A. A. Wragg, *Trans. Instn. Chem. Engrs* **57** (1979) 176.
[2] K. M. Krall and E. M. Sparrow, *J. Heat Transfer* **88** (1966) 131.
[3] S. M. Chouikhi, PhD Thesis, University of Exeter (1985).
[4] S. M. Chouikhi, M. A. Patrick and A. A. Wragg, Proc. Int. Conf. Physical Modelling of Multi-phase Flow, Coventry, UK, (April 1983), p. 53ff.
[5] *Idem*, Proc. 3rd Int. Conf. Multi-phase Flow, The Hague, Netherlands, May 1987.
[6] A. K. Runchal, *Int. J. Heat Mass Transfer* **14** (1971) 781.
[7] T. Sydberger and U. Lotz, *J. Electrochem. Soc.* **129** (1982) 276.
[8] J. B. Harris, PhD Thesis, University of Exeter (1987).

[9] S. J. Wilkin and H. W. K. Cheung, Central Electricity Research Laboratories, Leatherland, UK, Report No. TPRD/L/E 500051/M82 (1982).
[10] B. Poulson and R. Robinson, *Corros. Sci.* **26** (1986) 265.
[11] A. A. Wragg, D. J. Tagg and M. A. Patrick, *J. Appl. Electrochem.* **10** (1980) 43.
[12] M. O. Awe, G. P. Hammond and J. Ward, Proc. 7th Int. Heat Transfer Conf., Munich (Sept. 1982) p. 15.
[13] B. Poulson, *Corros. Sci.* **23** (1983) 391.
[14] J. G. A. Pembery, PhD Thesis, University of Exeter (1985).
[15] A. A. Wragg, *Chem. Engr.* **316** (1977) 39.
[16] J. R. Selman and C. W. Tobias, *Adv. Chem. Eng.* **10** (1978) 211.
[17] F. P. Berger and K-F. F-L. Hau, *Int. J. Heat Mass Transfer* **20** (1977) 1185.